Article:
Auer, S orcid.org/0000-0003-0418-1745 and Kashchiev, D (2022) Two-step crystal nucleation kinetics: Solution of the master equation. Journal of Crystal Growth, 580. 126469. ISSN 0022-0248

https://doi.org/10.1016/j.jcrysgro.2021.126469

SUPPLEMENTARY MATERIAL

Two-Step Crystal Nucleation Kinetics: Solution of the Master Equation

Stefan Auer [a] and Dimo Kashchiev [b]

[a] *School of Chemistry, University of Leeds, Leeds LS2 9JT, United Kingdom*
[b] *Institute of Physical Chemistry, Bulgarian Academy of Sciences, ul. Acad. G. Bonchev 11, Sofia 1113, Bulgaria*

E-mail addresses:
[a] s.auer@leeds.ac.uk
[b] kash@ipc.bas.bg

Contents

Below, some issues in the main text (MT) of the paper are further discussed and additional data from our numerical study of two-step (2S) crystal nucleation are presented.

S1. Fluxes, formation work, and attachment/detachment frequencies

The three cluster fluxes $I_{i,n}$, $G_{i,n}$ and $K_{i,i}$ in eqs. (1)–(3) and in Fig. 1b of MT are given by [1]

$$I_{i,n} = f_{i,n} C_{i,n} \left(\frac{Z_{i,n}}{C_{i,n}} - \frac{Z_{i+1,n}}{C_{i+1,n}} \right) \tag{S1}$$

$$G_{i,n} = g_{i,n} C_{i,n} \left(\frac{Z_{i,n}}{C_{i,n}} - \frac{Z_{i,n+1}}{C_{i,n+1}} \right) \tag{S2}$$

$$K_{i,i} = k_{i,i} C_{i,i} \left(\frac{Z_{i,i}}{C_{i,i}} - \frac{Z_{i+1,i+1}}{C_{i+1,i+1}} \right) \tag{S3}$$

and are analogous to the sole cluster flux in Classical Nucleation Theory (CNT) [2]. As illustrated in Fig. 1a of MT, $f_{i,n}$ (s^{-1}) and $g_{i,n}$ (s^{-1}) are the attachment frequencies, respectively, of monomers of the old phase (O-phase) to the surface of an i,n-sized composite and of monomers of the metastable-phase (M-phase) layer of such composite to the surface of the n-sized crystal in it, and $k_{i,i}$ (s^{-1}) is the attachment frequency of those monomers of the O-phase to the surface of an i-sized crystal in the O-phase (i.e. of an i,i-sized cluster) that transform it into a crystal of size $i+1$. Also, $C_{i,n}$ (m^{-3}) is the equilibrium concentration of i,n-sized clusters and $Z_{i,n}$ (m^{-3}) is the actual concentration of these clusters.

All three fluxes depend exponentially on the dimensionless work $w_{i,n}$ to form an i,n-sized cluster, because $C_{i,n}$ is related to $w_{i,n}$ by the Boltzmann-type formula [1] ($i = 1,2,3,\ldots$, $n = 1,2,3,\ldots,i$)

$$C_{i,n} = C_1 \exp(w_{1,1} - w_{i,n}) \tag{S4}$$

in which C_1 is the concentration of monomers in the O-phase, and $w_{1,1}$ is the value of $w_{i,n}$ at $i = n = 1$. Equation (S4) is self-consistent in the sense that at $i = n = 1$ it returns the equality $C_{1,1} = C_1$. Also, it is general and can be used with any model for $w_{i,n}$. The simplest expression for $w_{i,n}$ is of the form [1] ($i = 1,2,3,\ldots$, $n = 1,2,3,\ldots,i$, $s_{co} > s_{cm} > 0$)

$$w_{i,n} = -(s_{co} - s_{cm})i + \gamma_{mo} i^{2/3} - s_{cm} n + \gamma_{cm} n^{2/3} \tag{S5}$$

where $s_{co} - s_{cm} = s_{mo}$ is the dimensionless supersaturation of the O-phase with respect to the M-phase, s_{co} is the dimensionless supersaturation of the O-phase with respect to the crystal phase (C-phase), s_{cm} is the dimensionless supersaturation of the M-phase with respect to the C-phase, γ_{mo} is the dimensionless M-phase/O-phase specific surface energy, and γ_{cm} is the dimensionless C-phase/M-phase specific surface energy.

When the O-phase is a single-component vapor behaving as ideal gas, the three supersaturations are given by [1]

$$s_{co} = \ln\left(\frac{p}{p_{e,c}} \right), \qquad s_{mo} = \ln\left(\frac{p}{p_{e,m}} \right), \qquad s_{cm} = \ln\left(\frac{p_{e,m}}{p_{e,c}} \right) \tag{S6}$$

where p is the actual pressure of the O-phase monomers, and $p_{e,m}$ and $p_{e,c}$ are their saturation pressures over the bulk M-phase and C-phase, respectively. Expressions for the above three supersaturations in the case of O-phase which is a single-component melt are presented elsewhere [1],[3]. It is important to note that s_{cm} is independent of s_{co} when s_{co} is changed via

p. When both the M-phase and the C-phase clusters are treated as spherical, for γ_{mo} and γ_{cm} we have [1]

$$\gamma_{mo} = \frac{(36\pi v_0^2)^{1/3}\sigma_{mo}}{k_B T}, \qquad \gamma_{cm} = \frac{(36\pi v_0^2)^{1/3}\sigma_{cm}}{k_B T} \tag{S7}$$

where σ_{mo} (J m^{-2}) and σ_{cm} (J m^{-2}) are the specific M-phase/O-phase and C-phase/M-phase surface energies, respectively, v_0 is the monomer volume, k_B is the Boltzmann constant, and T is the absolute temperature of the system. Also, due to the assumed spherical shape of the clusters, γ_{mo} and γ_{cm} are related to the dimensionless C-phase/O-phase specific surface energy γ_{co} by the simple equality [1]

$$\gamma_{co} = \gamma_{cm} + \gamma_{mo} \tag{S8}$$

in which γ_{co} is defined as (σ_{co} (J m^{-2}) is the specific C-phase/O-phase surface energy)

$$\gamma_{co} = \frac{(36\pi v_0^2)^{1/3}\sigma_{co}}{k_B T}. \tag{S9}$$

Besides thermodynamics (via $w_{i,n}$), kinetics is also involved in the $I_{i,n}$, $G_{i,n}$ and $K_{i,i}$ fluxes through the monomer attachment frequencies $f_{i,n}$, $g_{i,n}$ and $k_{i,i}$. For the simplest version of the composite-cluster model used by us, provided all monomers arriving at the cluster surface are attached to the cluster, we can approximate the i,n dependence of these frequencies by the CNT expressions for 1S nucleation [1],[2]

$$f_{i,i} = (1-Q) f_0 e^{s_{co}} i^{2/3}, \; f_{i,n} = f_0 e^{s_{co}} i^{2/3} \; (\text{for } n < i) \tag{S10}$$

$$g_{i,n} = g_0 e^{s_{cm}} n^{2/3} \; (\text{for } n < i) \tag{S11}$$

$$k_{i,i} = Q f_0 e^{s_{co}} i^{2/3}. \tag{S12}$$

These expressions correspond to the case of monomer attachment to the clusters in the gaseous O-phase by direct impingement onto the cluster surface and to monomer attachment to the crystals within the composites by interface-transfer control. In this case, when all clusters are spherical and the M-phase is a melt, for the frequency factors f_0 (s^{-1}) and g_0 (s^{-1}) we have [1]

$$f_0 = \frac{(36\pi v_0^2)^{1/3} p_{e,c}}{(2\pi m_0 k_B T)^{1/2}}, \quad g_0 = \frac{k_B T e^{-\lambda}}{3 v_0 \eta}. \tag{S13}$$

Here m_0 is the monomer mass, η is the viscosity of the melt (the M-phase) surrounding the crystal within a composite, $\lambda = l_m / k_B T$, and l_m is the per-monomer latent heat of melting of this crystal. As to the factor Q in eqs. (S10) and (S12), it is that fraction of O-phase monomers attached to an i,i-sized crystal in the O-phase, which is responsible for the growth of this crystal to an $i+1,i+1$-sized one. The $Q = 0$ limit implies neither growth of the i,i-sized crystals to $i+1,i+1$-sized ones nor decay of the latter into the former (no $k_{i,i}$ and $K_{i,i}$ arrows in Fig. 1 of MT). Similarly, in the $Q = 1$ limit, neither transition of the i,i-sized crystals to $i+1,i$-sized composites nor the opposite transition is possible (no $f_{i,i}$ and $I_{i,i}$ arrows in Fig. 1 of MT). According to eqs. (S10) and (S12), $f_{i,i}$ and $k_{i,i}$ are interrelated by the equation $f_{i,i} + k_{i,i} = f_0 e^{s_{co}} i^{2/3}$ so that, as it should be, all i-sized clusters in the O-phase (droplets, composites, and crystals) attach the same number of O-phase monomers per unit time ($f_0 e^{s_{co}} i^{2/3}$ in our case), because they have the same surface area.

S2. Master equation

When s_{co} and T are fixed, $C_{i,n}$ is time-independent so that using eqs. (S1)–(S3) in eqs. (1)–(3) of MT results in ($i = 3,4,...,M-1$, $n = 2,3,...,i-1$)

$$\frac{d}{dt}\left(\frac{Z_{i,n}}{C_{i,n}}\right) = f_{i-1,n}\frac{C_{i-1,n}}{C_{i,n}}\left(\frac{Z_{i-1,n}}{C_{i-1,n}} - \frac{Z_{i,n}}{C_{i,n}}\right) - f_{i,n}\left(\frac{Z_{i,n}}{C_{i,n}} - \frac{Z_{i+1,n}}{C_{i+1,n}}\right) + g_{i,n-1}\frac{C_{i,n-1}}{C_{i,n}}\left(\frac{Z_{i,n-1}}{C_{i,n-1}} - \frac{Z_{i,n}}{C_{i,n}}\right) - g_{i,n}\left(\frac{Z_{i,n}}{C_{i,n}} - \frac{Z_{i,n+1}}{C_{i,n+1}}\right) \tag{S14}$$

and in ($i = 2,3,...,M-1$)

$$\frac{d}{dt}\left(\frac{Z_{i,1}}{C_{i,1}}\right) = f_{i-1,1}\frac{C_{i-1,1}}{C_{i,1}}\left(\frac{Z_{i-1,1}}{C_{i-1,1}} - \frac{Z_{i,1}}{C_{i,1}}\right) - f_{i,1}\left(\frac{Z_{i,1}}{C_{i,1}} - \frac{Z_{i+1,1}}{C_{i+1,1}}\right) - g_{i,1}\left(\frac{Z_{i,1}}{C_{i,1}} - \frac{Z_{i,2}}{C_{i,2}}\right) \tag{S15}$$

$$\frac{d}{dt}\left(\frac{Z_{i,i}}{C_{i,i}}\right) = k_{i-1,i-1}\frac{C_{i-1,i-1}}{C_{i,i}}\left(\frac{Z_{i-1,i-1}}{C_{i-1,i-1}} - \frac{Z_{i,i}}{C_{i,i}}\right) - k_{i,i}\left(\frac{Z_{i,i}}{C_{i,i}} - \frac{Z_{i+1,i+1}}{C_{i+1,i+1}}\right) + g_{i,i-1}\frac{C_{i,i-1}}{C_{i,i}}\left(\frac{Z_{i,i-1}}{C_{i,i-1}} - \frac{Z_{i,i}}{C_{i,i}}\right) - f_{i,i}\left(\frac{Z_{i,i}}{C_{i,i}} - \frac{Z_{i+1,i}}{C_{i+1,i}}\right). \tag{S16}$$

To numerically solve these three equations (in which t is time and M is the number of O-phase monomers), it is convenient to combine them into a single equation of the form ($i = 2,3,...,M-1$, $n = 1,2,...,i$)

$$\frac{dF_{i,n}}{dx} = a_{i,n}(F_{i-1,n} - F_{i,n}) - b_{i,n}(F_{i,n} - F_{i+1,n}) + c_{i,n}(F_{i,n-1} - F_{i,n}) - d_{i,n}(F_{i,n} - F_{i,n+1}) + e_{i,n}(F_{i-1,i-1} - F_{i,i}) - h_{i,n}(F_{i,i} - F_{i+1,i+1}). \tag{S17}$$

This equation is eq. (6) of MT, and in it the unknown function $F_{i,n}$ is defined by

$$F_{i,n}(x) = \frac{Z_{i,n}(x)}{C_{i,n}}, \tag{S18}$$

$x = f_0 t$ is dimensionless time, and f_0 (s^{-1}) is a suitably chosen frequency parameter. Due to eq. (S4) for $C_{i,n}$, the x-independent dimensionless attachment ($b_{i,n}$, $d_{i,n}$, $h_{i,n}$) and detachment ($a_{i,n}$, $c_{i,n}$, $e_{i,n}$) frequencies read

$$a_{i,i} = 0,\ a_{i,n} = (f_{i-1,n}/f_0)\exp(w_{i,n} - w_{i-1,n}) \text{ (for } n < i) \tag{S19}$$

$$b_{i,n} = f_{i,n}/f_0 \text{ (for } n \le i) \tag{S20}$$

$$c_{i,1} = 0,\ c_{i,n} = (g_{i,n-1}/f_0)\exp(w_{i,n} - w_{i,n-1}) \text{ (for } 2 \le n \le i) \tag{S21}$$

$$d_{i,i} = 0,\ d_{i,n} = g_{i,n}/f_0 \text{ (for } n < i) \tag{S22}$$

$$e_{i,n} = 0 \text{ (for } n < i),\ e_{i,i} = (k_{i-1,i-1}/f_0)\exp(w_{i,i} - w_{i-1,i-1}) \tag{S23}$$

$$h_{i,n} = 0 \text{ (for } n < i),\ h_{i,i} = k_{i,i}/f_0. \tag{S24}$$

Equations (S17)–(S24) are general in the sense that they are in force for any model for the cluster formation work and the monomer attachment frequencies. With our model

expressions for $w_{i,n}$, $f_{i,n}$, $g_{i,n}$ and $k_{i,i}$, eqs. (S5) and (S10)–(S12), eqs. (S19)–(S24) become the equations used by us in solving eq. (S17) ($s_{co} > s_{cm} > 0$)

$$a_{i,i} = 0\,,\ a_{i,i-1} = (1-Q)(i-1)^{2/3}\exp\{s_{cm} + \gamma_{mo}[i^{2/3} - (i-1)^{2/3}]\} \tag{S25}$$

$$a_{i,n(n<i-1)} = (i-1)^{2/3}\exp\{s_{cm} + \gamma_{mo}[i^{2/3} - (i-1)^{2/3}]\} \tag{S26}$$

$$b_{i,i} = (1-Q)i^{2/3}\exp(s_{co})\,,\ b_{i,n(n<i)} = i^{2/3}\exp(s_{co}) \tag{S27}$$

$$c_{i,n(n\le i)} = L(n-1)^{2/3}\exp\{\gamma_{cm}[n^{2/3} - (n-1)^{2/3}]\} \tag{S28}$$

$$d_{i,i} = 0\,,\ d_{i,n(n<i)} = Ln^{2/3}\exp(s_{cm}) \tag{S29}$$

$$e_{i,n(n<i)} = 0\,,\ e_{i,i} = Q(i-1)^{2/3}\exp\{\gamma_{co}[i^{2/3} - (i-1)^{2/3}]\} \tag{S30}$$

$$h_{i,n(n<i)} = 0\,,\ h_{i,i} = Qi^{2/3}\exp(s_{co}) \tag{S31}$$

($L = g_0 / f_0 \ge 0$ is a numerical factor with f_0 and g_0 given by eq. (S13)). It is seen from these equations that, as the system temperature is fixed, the experimentally controlled supersaturation s_{co} only affects $b_{i,i}$, $b_{i,n(n<i)}$ and $h_{i,i}$ (i.e. the monomer attachment solely to the clusters in the O-phase), because s_{cm} does not change with changing s_{co}.

S3. Parameter values

Our task is to numerically solve the master equation (S17) for $F_{i,n}(x)$ when the attachment/detachment frequencies from eqs. (S25)–(S31) are approximately relevant to homogeneous nucleation of water droplets (the M-phase) and ice crystals (the C-phase) in steam (the O-phase) at temperature $T \approx 220 - 230$ K and of ice crystals in liquid water at the same temperature. In this case, we have $p_{e,c} \approx 5$ Pa and $p_{e,m} \approx 8$ Pa [4], $\sigma_{co} \approx 106$ mJ m^{-2}, $\sigma_{mo} \approx 88$ mJ m^{-2} and $\sigma_{cm} \approx 18$ mJ m^{-2} (Ref. [5], p. 160), and $\eta \approx 0.07$ Pa s (from eq. (13.47) of Ref. [2]). Also, as for water $m_0 \approx 3\times10^{-26}$ kg, $v_0 \approx 3\times10^{-29}$ m^3 and $l_m \approx 10^{-20}$ J, from eqs. (S6), (S7), (S9) and (S13) we find $s_{cm} = 0.5$, $\gamma_{mo} = 12.8$, $\gamma_{cm} = 2.6$, $\gamma_{co} = 15.4$, $f_0 = 10^5$ s^{-1}, and $g_0 = 2\times10^7$ s^{-1}. Regarding C_1, we use $C_1 = 1.6\times10^{21}e^{s_{co}}$ m^{-3} which follows from $C_1 = p/k_BT$ and $p = p_{e,c}e^{s_{co}}$ (this formula for C_1 represents the ideal-gas equation of state $p = C_1k_BT$ in which $C_1 = N_1/V$ is the monomer concentration, N_1 is the number of gas molecules, and V is the gas volume). As seen, the three γ's satisfy eq. (S8). Also, for the ratio $L = g_0/f_0$ we have $L = 200$. This means that when s_{co} is sufficiently small, monomer attachment to an n-sized ice crystal inside a water composite of $i > n$ monomers can be much faster than that to the liquid layer of the composite or to a droplet of the same size i as long as i is not too much greater than n (see eqs. (S10) and (S11)). As to the parameter Q, its value is unknown and we choose $Q = 1/2$, the value corresponding to equal frequencies $f_{i,i}$ and $k_{i,i}$ of monomer attachment to equisized water droplets and ice crystals in the steam (see eqs. (S10) and (S12)).

S4. Nonstationary nucleation rates

The nonstationary nucleation rates J_{d+com} of $i > i^*$-sized droplets plus composites, J_{com} of $i > i^*$-sized composites, $J_{d+com+c}$ of $i > i^*$-sized droplets plus $i > i^*$-sized composites plus $i > i_{co}^*$-sized crystals, $J_{c,1S}$ of 1S nucleation of $i > i_{co}^*$-sized ice crystals in the O-phase, and $J_{d,1S}$ of 1S droplet nucleation are given by [1]

$$J_{d+com}(t) = \sum_{n=1}^{i^*} I_{i^*,n} + \sum_{i=i^*+1}^{M-1} \left(I_{i,i} - G_{i,i-1} \right) \tag{S32}$$

$$J_{com}(t) = J_{d+com} - J_d = \sum_{n=2}^{i^*} I_{i^*,n} + \sum_{i=i^*+1}^{M-1} \left(I_{i,i} - G_{i,i-1} + G_{i,1} \right) \tag{S33}$$

$$J_{d+com+c}(t) = J_{d+com} + J_c . \tag{S34}$$

$$J_{c,1S}(t) = K_{i_{co}^*, i_{co}^*} \text{ (at } Q = 1 \text{ and } a_{i,n} = b_{i,n} = c_{i,n} = d_{i,n} = 0 \text{)} \tag{S35}$$

$$J_{d,1S}(t) = I_{i^*,1} \text{ (at } Q = c_{i,n} = d_{i,n} = e_{i,n} = h_{i,n} = 0 \text{).} \tag{S36}$$

Here J_c and J_d, specified by eqs. (12) and (14) of MT, are the 2S nucleation rates of, respectively, crystals and droplets in the O-phase. Also, $I_{i^*,n}$, $I_{i,i}$, $G_{i,i-1}$, $G_{i,1}$, $K_{i_{co}^*, i_{co}^*}$, and $I_{i^*,1}$ are cluster fluxes defined by eqs. (S1)–(S3), i^* is the size of the droplet nucleus, and i_{co}^* is the size of the crystal nucleus in the O-phase. It should be noted that unlike in Ref. [1] in which the droplets and the composites are collectively called "composites" so that their nucleation rate is given by eq. (S32), in the present paper the composites are regarded as distinct from the droplets and, accordingly, J_{com} is determined by eq. (S33). The rate $J_{c,1S}$ is obtained from the solution of eq. (S17) at $Q = 1$ and $a_{i,n}$, $b_{i,n}$, $c_{i,n}$ and $d_{i,n}$ set equal to zero and corresponds to the CNT 1S process of droplet-unaffected crystal nucleation in the one-dimensional cluster size space of the $n = i$ diagonal in Fig. 1b of MT. Similarly, the rate $J_{d,1S}$ is obtained from the solution of eq. (S17) at annulled Q, $c_{i,n}$, $d_{i,n}$, $e_{i,n}$, and $h_{i,n}$. This is the rate of the CNT 1S process of crystal-unaffected droplet nucleation in the one-dimensional cluster size space of the i axis in Fig. 1b of MT (then no ice crystals nucleate in either the O-phase or the droplets).

Figure S1 displays the time dependences of the nucleation rates from eqs. (S32)–(S34) and from eq. (14) of MT at $s_{co} = 2.5$, 3 and 5 (panels (a), (b) and (c), respectively). We see that at these three supersaturations: (i) all these rates have the sigmoidal shape known from the CNT 1S nucleation [2], but J_d has an almost imperceptible maximum before attaining stationarity; (ii) J_d is only a little greater than J_{com}; and (iii) J_{d+com} (solid line) is practically equal to $J_{d+com+c}$ (dashed line) because of the negligible contribution of the 2S crystal nucleation rate J_c from eq. (12) of MT to the droplet and composite nucleation rates.

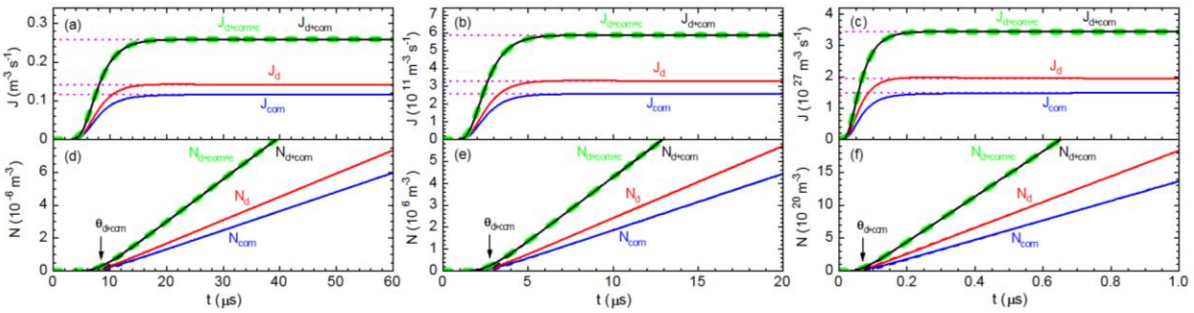

Figure S1. Time dependence of the nucleation rates J and the number densities N of supernuclei (as indicated) from eqs. (S32)–(S34) and eq. (14) of MT, and from eqs. (S41) and (S43) at $s_{co} = 2.5$ (left panels), $s_{co} = 3$ (middle panels), and $s_{co} = 5$ (right panels). The dotted lines in the $J(t)$ panels represent the respective stationary nucleation rates, the thin dashed lines in the $N(t)$ panels are the long-time $N(t)$ asymptotes, and the arrows in these panels indicate the delay time θ_{d+com} of droplet-plus-composite nucleation. The thick dashed lines graph $J_{d+com+c}$ and $N_{d+com+c}$.

S5. Stationary nucleation rates

The stationary nucleation rates J^s_{d+com} of $i > i^*$-sized droplets plus composites, J^s_{com} of $i > i^*$-sized composites, and $J^s_{d+com+c}$ of $i > i^*$-sized droplets plus $i > i^*$-sized composites plus $i > i_{co}{}^*$-sized crystals are the $t \to \infty$ values of J_{d+com}, J_{com} and $J_{d+com+c}$ from eqs. (S32)–(S34). Figure S2 exhibits the supersaturation dependence of these rates and of the stationary rate J^s_d of droplet nucleation from eq. (14) of MT. It is seen that J^s_{com}, J^s_{d+com} and $J^s_{d+com+c}$ are practically equal to each other and that J^s_d is also equal to them except for $s_{co} \le 2.2$. The inset in Fig. S2 shows that at these low supersaturations the nucleation rate of the composites can be orders of magnitude higher than the droplet nucleation rate.

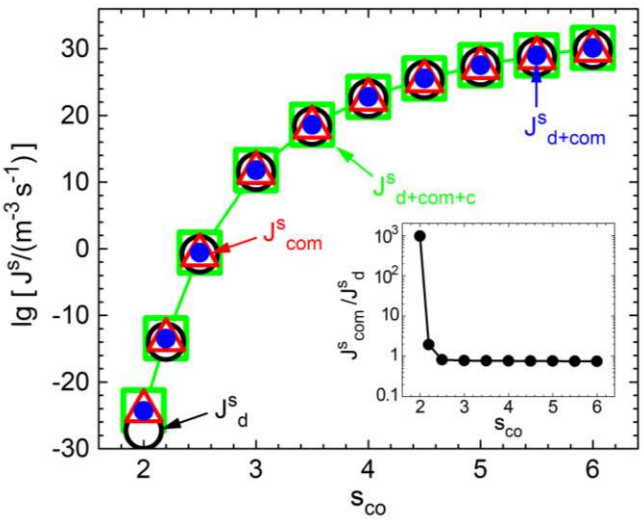

Figure S2. Supersaturation dependence of the stationary nucleation rates J^s_{com}, J^s_{d+com}, and $J^s_{d+com+c}$ from eqs. (S32)–(S34) and J^s_d from eq. (14) of MT (as indicated). The inset illustrates the ratio between the composite and the droplet stationary nucleation rates, and the lines are drawn to guide the eye.

Table S1 presents numerically the supersaturation dependence of all stationary nucleation rates obtained in our study from eqs. (12)–(14) of MT and eqs. (S32)–(S36) (graphically, these dependences are shown in Fig. 6 of MT and Fig. S2 above). In the table, "lg" denotes the base-10 (a.k.a. common) logarithm.

Table S1. Dependence of stationary nucleation rates J^s (m^{-3} s^{-1}) on the supersaturation s_{co} at $M = 240$.

s_{co}	lg J^s_c	lg $J^s_{c,1S}$	lg $J^s_{c,d}$	lg J^s_d	lg $J^s_{d,1S}$	lg J^s_{com}	lg J^s_{d+com}	lg $J^s_{d+com+c}$
2.0	–25.332	–25.118	–24.077	–27.312	–27.292	–24.327	–24.326	–24.286
2.2	–14.889	–14.836	–13.873	–13.943	–13.926	–13.654	–13.474	–13.457
2.5	–3.177	–3.753	–2.101	–0.849	–0.840	–0.933	–0.588	–0.587
3.0	8.498	7.953	9.745	11.517	11.521	11.411	11.769	11.769
3.5	14.630	15.096	16.255	18.330	18.334	18.220	18.580	18.580
4.0	17.561	19.809	20.170	22.522	22.528	22.410	22.771	22.771
4.5	17.883	23.107	22.648	25.316	25.326	25.201	25.563	25.563
5.0	15.525	25.529	24.220	27.290	27.312	27.173	27.537	27.537
5.5	14.418	27.377	25.100	28.754	28.794	28.634	28.999	28.999
6.0	15.643	28.834	25.223	29.880	29.947	29.756	30.124	30.124

To determine the stationary rate $J^s_{c,d,dis}$ of crystal nucleation in dispersed $Z^s_{i,1}$ droplets, which is displayed in Fig. 6b of MT, we need the stationary rate $J^s_{c,d,\infty}$ of homogeneous nucleation of crystals in the bulk M-phase (a macroscopically large droplet). This rate is given exactly by the Becker-Döring formula [2],[6] $J^s_{c,d,\infty} = 1/\sum_{n=1}^{\infty}(1/g_n C_n)$. Here $C_n = C_0 \exp(-w_n)$ is the equilibrium concentration of n-sized crystals in the M-phase, $C_0 = 1/v_0$ is the concentration of nucleation sites in this phase [2], v_0 is the monomer volume, $w_n = -s_{cm} n + \gamma_{cm} n^{2/3}$ is the work to form an n-sized crystal in this phase [2], and the attachment frequency g_n is the frequency $g_{i,n}$ specified by eq. (S11). The rate $J^s_{c,d,\infty}$ is thus s_{co}-independent and can be presented as

$$J^s_{c,d,\infty} = \frac{f_0}{v_0}\left(\sum_{n=1}^{\infty}\frac{e^{w_n}}{d_n}\right)^{-1} \tag{S37}$$

where d_n is the frequency $d_{i,n}$ given by eq. (S29). The crystal nucleation rate within an i-sized M-phase cluster (water droplet in our case) with volume $v_0 i$ is the product $J^s_{c,d,\infty} v_0 i$ so that $Z^s_{i,1}$ such clusters nucleate crystals at rate $J^s_{c,d,\infty} v_0 i Z^s_{i,1}$ ($Z^s_{i,1}$ is the stationary concentration of i-sized M-phase clusters, see Figs. 3d–3f of MT). Hence, the stationary nucleation rate $J^s_{c,d,dis}$ of crystals in the dispersion of M-phase clusters capable of nucleating crystals is the sum of $J^s_{c,d,\infty} v_0 i Z^s_{i,1}$ over the size i of these clusters. For small s_{co} values we have $i^* \geq n^*$ so that all M-phase supernuclei of size $i \geq i^*+1$ can nucleate crystals (to a certain approximation, the $i \leq i^*$-sized M-phase clusters can be neglected because of their tendency to decay). However, when the supersaturation s_{co} is so high that $i^* < n^*$, crystals can be nucleated only within the M-phase supernuclei of size $i \geq n^*+1$. Therefore, using $J^s_{c,d,dis}$ from eq. (S37) in the product $J^s_{c,d,\infty} v_0 i Z^s_{i,1}$ and summing over i leads to

$$J^s_{c,d,dis} = f_0\left(\sum_{n=1}^{\infty}\frac{e^{w_n}}{d_n}\right)^{-1}\sum_{i=j^*+1}^{M-1} i Z^s_{i,1} \tag{S38}$$

where $j^* = i^*$ when $i^* \geq n^*$ (small s_{co}, in our case $s_{co} \leq 3$) or $j^* = n^*$ when $i^* < n^*$ (large s_{co}, in our case $s_{co} > 3$). It is important to note that, in contrast to $J^s_{c,d,\infty}$, $J^s_{c,d,dis}$ depends on s_{co} due to the change of both i^* and $Z^s_{i,1}$ with s_{co}.

Our numerical results for the stationary rates $J^s_{c,1S}$ and $J^s_{d,1S}$ of 1S crystal and droplet nucleations (Figs. 6a and 6c of MT) can be verified with the aid of the exact Becker-Döring formula [2],[6] which in our case is of the form $J^s_{c,1S} = 1/\sum_{i=1}^{M-1}(1/k_{i,i}C_{i,i})$ for 1S crystal nucleation and $J^s_{d,1S} = 1/\sum_{i=1}^{M-1}(1/f_{i,1}C_{i,1})$ for 1S (i.e. crystal-unaffected) droplet nucleation. Owing to eq. (S4), we therefore have

$$J^s_{c,1S} = f_0 C_1\left(\sum_{i=1}^{M-1}\frac{e^{w_{i,i}-w_{1,1}}}{h_{i,i}}\right)^{-1}, \quad J^s_{d,1S} = f_0 C_1\left(\sum_{i=1}^{M-1}\frac{e^{w_{i,1}-w_{1,1}}}{b_{i,1}}\right)^{-1}. \tag{S39}$$

Here $h_{i,i}$ and $b_{i,1}$ are given by eqs. (S31) and (S27), the former with $Q=1$ and the latter with $Q=0$, because $J^s_{c,1S}$ and $J^s_{d,1S}$ are 1S nucleation rates. With $f_0=10^5$ s^{-1} and $C_1=1.6\times10^{21}e^{s_{co}}$ m^{-3} from Section S3 and with $w_{i,i}$, $w_{i,1}$ and $w_{1,1}$ from eq. (S5), the above equations yield $J^s_{c,1S}$ and $J^s_{d,1S}$ values which for all supersaturations are equal to those from the solution of eq. (S17).

S6. The J^s_c components

According to eq. (12) of MT, the stationary rate J^s_c of 2S crystal nucleation is given by $J^s_c=K^s+G^s-I^s$. Here $K^s\equiv K^s_{i_{co}*,i_{co}*}$ is the stationary flux of crystals on the $n=i$ diagonal in the cluster size space (Fig. 1b of MT), $G^s\equiv\sum_{i=i_{co}*+1}^{M-1}G^s_{i,i-1}$ is the collective stationary flux of crystallizing composites, and $I^s\equiv\sum_{i=i_{co}*+1}^{M-1}I^s_{i,i}$ is the collective stationary flux of crystals that become composites. The supersaturation dependence of these three J^s_c components is illustrated in Fig. S3 by diamonds (component K^s), circles (component G^s) and squares (component I^s). We see that all components increase monotonically with s_{co} and that I^s becomes greater than G^s for $s_{co}\geq3.5$. As a result, the G^s-I^s term in the above equation for J^s_c becomes negative so that it subtracts from K^s, and this makes J^s_c orders of magnitude smaller than K^s in the range of high supersaturations. The down triangles in Fig. 3S illustrate the $J^s_c(s_{co})$ dependence from the above equation for J^s_c (this dependence is also shown in Fig. 6a of MT).

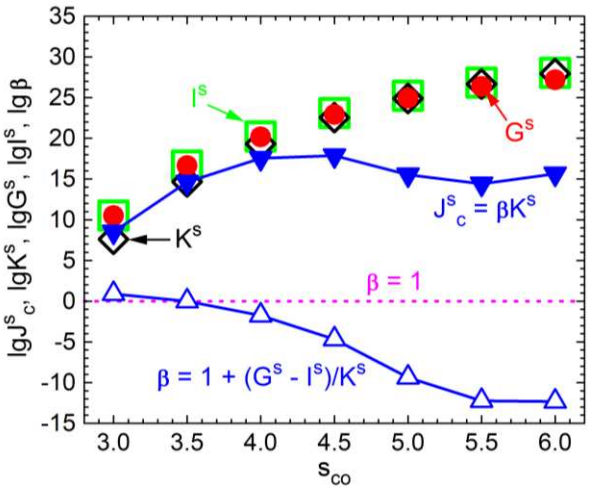

Figure S3. Supersaturation dependence of the numerically obtained stationary 2S crystal nucleation rate J^s_c (down triangles), of its three components K^s (diamonds), G^s (circles) and I^s (squares), and of the numerical factor β (up triangles). The solid lines are drawn to guide the eye, and the rate J^s_c and its components are in m^{-3} s^{-1}.

As G^s and I^s characterize 2S nucleation (they are nil in 1S crystal nucleation which evolves only on the $n = i$ line of the cluster size space, the diagonal in Fig. 1b of MT), to see their effect on J_c^s, it is convenient to represent J_c^s as $J_c^s = \beta K^s$ where $\beta = 1 + (G^s - I^s)/K^s$. The up triangles in Fig. S3 display the numerical factor β as a function of s_{co}. When $s_{co} > 3.5$, in absolute value, the negative flux difference $G^s - I^s$ is so very nearly equal to the positive flux K^s (up to 99.99999999999%) that this results in $\beta << 1$. We see in Fig. S3 that the strong drop of β below unity (the dotted line) for these high supersaturations is the reason for the orders-of-magnitude smallness of J_c^s in comparison with K^s. The decrease of β with s_{co} is initially so much faster than the increase of K^s that the increasing J_c^s passes trough a maximum and then starts decreasing with s_{co}. For $s_{co} \geq 5.5$, however, the decrease of β slows down, whereas K^s keeps rising quickly. As a result, after passing through a minimum, J_c^s resumes its increasing with s_{co}. It should be pointed out that, especially for $s_{co} \geq 3.5$, this behavior of J_c^s is influenced by the finite-size effect (see below) intrinsic to our results because of our use of $M = 240$ as the maximal cluster size in the numerical solution of the master equation of 2S nucleation.

S7. Effect of *M* on the stationary nucleation rates

In general, the value of the maximum cluster size *M* chosen when numerically solving the master equation of 2S nucleation, eq. (1) of MT, may have a considerable effect on the values of the various stationary nucleation rates characterizing the process. Our *M* value of 240 requires the numerical solution of $(M/2)(M-1) - 1 = 28679$ equations, and this large number prohibited us from using a considerably greater *M*. The size-effect due to our choice of $M = 240$ can be assessed at each supersaturation s_{co} by determining the various stationary nucleation rates at the smaller $M = 100$, 120, 160 and 200. It turns out that none of the rates J_d^s, J_{com}^s, J_{d+com}^s, $J_{d+com+c}^s$, $J_{c,1S}^s$ and $J_{d,1S}^s$ is significantly affected by these *M* values. Regarding J_c^s and $J_{c,d}^s$, however, the situation is quite different. As seen in Figs. S4a and S4c below, the size effect experienced by both these rates is relatively small when $M \geq 160$ and $s_{co} \leq 3.0$ (then $i^* \geq n^*$ so that the nucleation energy peak is inside the physically accessible triangular cluster-size space, Figs. 2a and 2b of MT). When $s_{co} > 3.0$, however, the effect of *M* on $J_{c,d}^s$ remains relatively small for $M \geq 160$, but on J_c^s it is considerable even at $M = 240$, the exception being the highest supersaturation (Figs. S4b and S4d). Interestingly, at many supersaturations, both $\lg J_c^s$ and $\lg J_{c,d}^s$ are nearly linear functions of $1/M$ when *M* is between 160 and 240. As the size effect is expected to disappear in the $M \to \infty$ limit, in trying to eliminate it, one could extrapolate the J_c^s-vs.-$1/M$ and the $J_{c,d}^s$-vs.-$1/M$ dependences up to $1/M = 0$, but we refrained from doing that because of the dubious validity of any extrapolation procedure, especially when the extrapolation range is too wide.

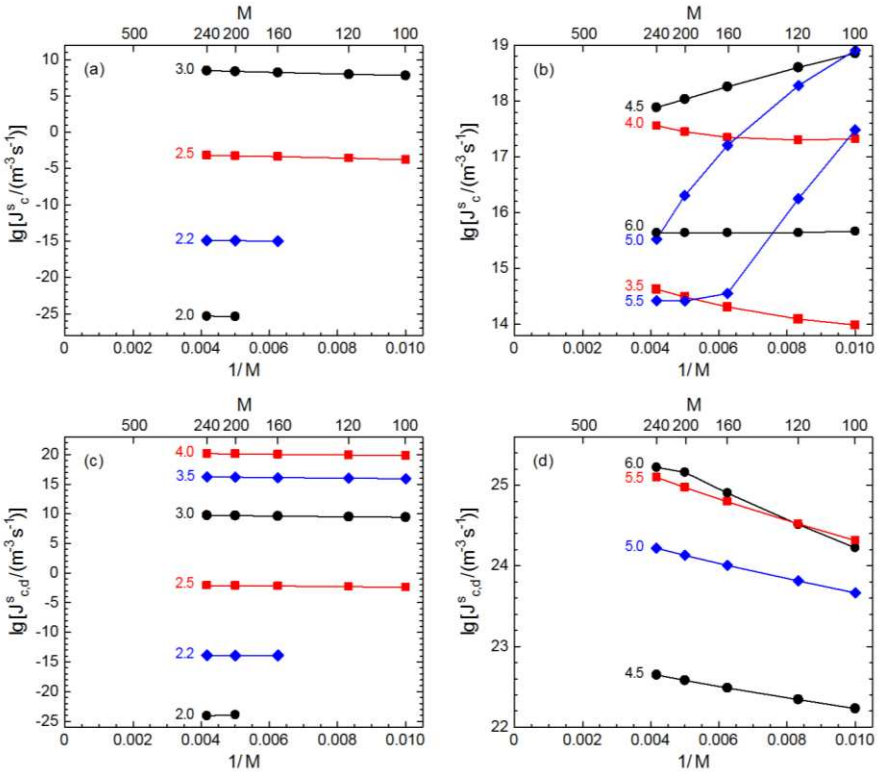

Figure S4. Dependence of the stationary 2S crystal nucleation rate J_c^s and the stationary rate $J_{c,d}^s$ of crystal nucleation in droplets on the maximum cluster size M used in solving the master equation of 2S nucleation, eq. (1) of MT. The symbols are our numerical data, the numbers indicate the supersaturations used in our study, and the lines are drawn to guide the eye.

S8. Relevance of our study to homogeneous nucleation of water droplets

As noted in Section 3.1 of MT, our study is only approximately relevant to homogeneous nucleation of water droplets (the M-phase) and ice crystals in steam (the O-phase) at a temperature T between 220 and 230 K. This is so mainly because experimentally obtained data for the crystal/vapor, crystal/liquid and liquid/vapor specific surface energies σ_{co}, σ_{cm} and σ_{mo} of water in this temperature range are either available solely from extrapolations (σ_{mo}) or are not available at all (σ_{co} and σ_{cm}). We used $\sigma_{mo} = 88$ mJ m^{-2} in our study, because in Ref. [5] (p. 160) this value is provided together with the σ_{co} and σ_{cm} values. For comparison, σ_{mo} values from extrapolation are [7] 84.25 mJ m^{-2} and 83.26 mJ m^{-2} at $T = 220$ and 230 K, respectively. Also, we used $p_{e,m} = 8$ Pa for the liquid/vapor saturation pressure, while $p_{e,m}$ values, also from extrapolation, are [7] 4.42 and 13.57 Pa at $T = 220$ and 230 K, respectively.

The open symbols in Fig. S5 display experimental data [8]–[11] (see also Fig. 5 of Ref. [7]) for the s_{mo} dependence of the stationary rate J_d^s of homogeneous nucleation of water droplets in steam at $T = 220$ and 230 K (as indicated). The supersaturation s_{mo} for droplet nucleation is experimentally controlled according to the relation $s_{mo} = \ln(p / p_{e,mo})$ in which p is the actual pressure of the steam. For comparison, the solid circles in Fig. S5 represent, in J_d^s-vs.-s_{mo} coordinates, our numerical data for J_d^s from Fig. 6c of MT (s_{mo} in Fig. S5 and s_{co} in Fig. 6c are interrelated by $s_{mo} = s_{co} - s_{cm}$, where from Section S3 we have $s_{cm} = 0.5$ in our case). As seen, qualitatively, our data are similar to the experimental ones. To visualize the discrepancy between experiment and CNT, the dashed lines in Fig. S5 graph the CNT formula for 1S droplet nucleation (e.g., eq. (20) of Ref. [7])

$$J_{d,CNT}^s = A_0 \exp\left(2s_{mo} - \frac{B}{s_{mo}^2}\right) \tag{S40}$$

in which the constants A_0 and B are specified [7] as $A_0 = 8.85 \times 10^{25}$ m^{-3} s^{-1} and $B = 348.9$ at $T = 220$ K and as $A_0 = 7.50 \times 10^{26}$ m^{-3} s^{-1} and $B = 287.3$ at $T = 230$ K. As pointed out in Section 4.5 of MT, our results for J_d^s indicate that this discrepancy is so large that it seems unlikely to be attributable to the rather weak effect of the 2S ice crystal nucleation on the droplet nucleation rate at these temperatures.

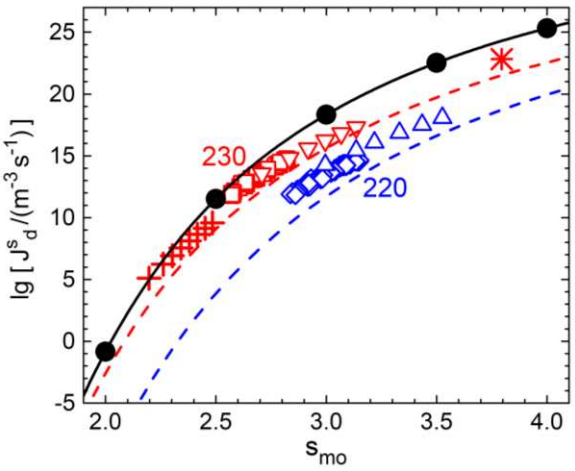

Figure S5. Supersaturation dependence of the stationary rate of homogeneous nucleation of water droplets in steam at $T = 220$ and 230 K (as indicated): circles – our numerical data from Fig. 6c of MT for the stationary nucleation rate J_d^s of water droplets involved in 2S ice crystal nucleation, diamonds (220 K) – data of Wölk and Strey [9], up triangles (220 K) – data of Holten et al. [11], squares (230 K) – data of Wölk and Strey [9], down triangles (230 K) – data of Holten et al. [11], pluses (230 K) – data of Miller et al. [8], star (230 K) – data of Kim et al. [10], dashed lines – eq. (S40) of CNT at 220 and at 230 K. The solid line is drawn to guide the eye.

S9. Number densities of supernuclei

In general, the number density N (m^{-3}) of any kind of supernuclei at time t is given by [2] $N(t)=\int_0^t J(t')dt'$. With the help of eqs. (12)–(14) of MT and eqs. (S32)–(S36), we therefore have

$$N_c(t)=\int_0^t J_c(t')dt',\ N_{c,d}(t)=\int_0^t J_{c,d}(t')dt',\ N_d(t)=\int_0^t J_d(t')dt' \tag{S41}$$

$$N_{c,1S}(t)=\int_0^t J_{c,1S}(t')dt',\ N_{d,1S}(t)=\int_0^t J_{d,1S}(t')dt' \tag{S42}$$

$$N_{com}(t)=\int_0^t J_{com}(t')dt',\ N_{d+com}(t)=\int_0^t J_{d+com}(t')dt',\ N_{d+com+c}(t)=\int_0^t J_{d+com+c}(t')dt'. \tag{S43}$$

These equations give the number densities N_c and $N_{c,1S}$ of 2S- and 1S-nucleated crystal supernuclei of size $i>i_{co}*$ in the O-phase, the number density $N_{c,d}$ of $n>n*$-sized crystal supernuclei in the composites of size $i\geq n*+1$, the number densities N_d and $N_{d,1S}$ of $i>i*$-sized supernucleus droplets (which in our case are the M-phase supernuclei) formed, respectively, in the course of 2S crystal nucleation and in the 1S process of droplet nucleation described by CNT, the number density N_{com} of $i>i*$-sized composites, the number densities N_{d+com} of $i>i*$-sized droplets plus composites, and the number density $N_{d+com+c}$ of $i>i*$-sized droplets plus $i>i*$-sized composites plus $i>i_{co}*$-sized crystals.

The time dependences of the last three number densities of supernuclei as well as of N_d from eq. (S41) are exhibited in Fig. S1 in which panels (d), (e) and (f) refer to $s_{co}=2.5$, 3 and 5, respectively. It is seen that all these dependencies have the long-time linear portion known from the CNT 1S nucleation [2] and allowing determination of the respective stationary nucleation rate and nucleation delay time. We observe also that at these supersaturations the droplets are only a little more numerous than the composites and that N_{d+com} (solid line) is practically equal to $N_{d+com+c}$ (thick dashed line) because of the negligible number density N_c of 2S-nucleated crystals.

S10. Nucleation delay times

The nucleation delay times θ_{d+com} of $i>i*$-sized droplets plus composites, θ_{com} of $i>i*$-sized composites, and $\theta_{d+com+c}$ of $i>i*$-sized droplets plus $i>i*$-sized composites plus $i>i_{co}*$-sized crystals are obtained from eq. (15) of MT in which t is a moment at which the nucleation is already stationary (e.g., the final moments of the $N_{d+com}(t)$, $N_{com}(t)$ and $N_{d+com+c}(t)$ curves in Fig. S1). The supersaturation dependence of these three delay times and of the delay time θ_d of 2S droplet nucleation from Fig. 7b of MT is presented in Fig. S6. We see that all delay times are practically equal to each other except for $s_{co}>5$. The inset of

Fig. S6 shows that for these high supersaturations θ_{com} is up to almost four-fold greater than θ_d. This is interesting vis-à-vis the finding that, again for these supersaturations, J^s_{com} and J^s_d are practically equal (see the inset of Fig. S2).

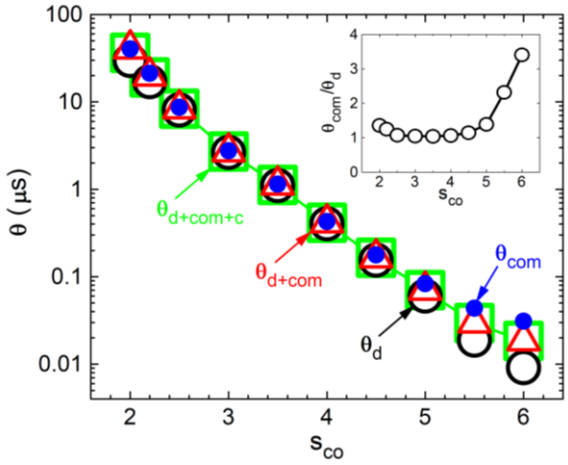

Figure S6. Supersaturation dependence of the nucleation delay times θ_{com} (solid circles), θ_{d+com} (triangles), $\theta_{d+com+c}$ (squares), and θ_d (open circles). The data are obtained from eq. (15) of MT, the inset illustrates the θ_{com}/θ_d ratio, and the lines are drawn to guide the eye.

Table S2 presents numerically the supersaturation dependence of all nucleation delay times obtained in our study from eq. (15) of MT (graphically, these dependences are shown in Fig. 7 of MT and Fig. S6 above). In the table, "*x*E*y*" stands for $x\times10^{y}$.

Table S2. Dependence of nucleation delay times θ (μs) on the supersaturation s_{co} at $M = 240$.

s_{co}	θ_c	$\theta_{c,1S}$	$\theta_{c,d}$	θ_d	$\theta_{d,1S}$	θ_{com}	θ_{d+com}	$\theta_{d+com+c}$
2.0	–4.79	19.3	–1.95E13	29.8	30.3	40.4	40.4	36.3
2.2	–1.99	12.1	–1.16E7	17.0	17.6	21.3	19.8	19.0
2.5	10.5	6.49	–16.8	8.09	8.33	8.68	8.36	8.36
3.0	7.00	2.47	9.13	2.64	2.69	2.77	2.69	2.70
3.5	2.16	0.971	4.74	1.10	1.11	1.15	1.12	1.12
4.0	–32.9	0.340	2.56	0.402	0.404	0.428	0.414	0.413
4.5	–1.05E4	0.145	1.47	0.155	0.155	0.177	0.165	0.164
5.0	–2.12E8	0.0720	0.886	0.0602	0.0622	0.0835	0.0703	0.0701
5.5	–7.08E10	0.0374	0.552	0.0189	0.0231	0.0437	0.0296	0.0294
6.0	–3.79E10	0.0251	0.335	0.00911	0.0139	0.0310	0.0185	0.0184

The CNT approximate general expression for the delay time of 1S nucleation, used in Section 4.7 of MT, is of the form

$$\theta = \frac{4m^*}{sf^*} \tag{S44}$$

where s is the dimensionless supersaturation, and f^* is the frequency of monomer attachment to nucleus of size m^*. In our case, $m^* = i_{co}^*$ and $s = s_{co}$ for the ice crystals in steam, whereas $m^* = i^*$ and $s = s_{mo} = s_{co} - s_{cm}$ for the droplets. Also, according to eq. (S12) with $Q = 1$ and eq. (S10) with $Q = 0$ (because $\theta_{c,1S}$ and $\theta_{d,1S}$ are 1S nucleation delay times), we have $f^* = f_0 e^{s_{co}} i_{co}^{*2/3}$ for these crystals and $f^* = f_0 e^{s_{co}} i^{*2/3}$ for the droplets. Hence, with the aid of the Gibbs-Thomson equations [1] $i_{co}^* = (2\gamma_{co}/3s_{co})^3$ and $i^* = [2\gamma_{mo}/3(s_{co} - s_{cm})]^3$, the above general expression for θ takes the form

$$\theta_{c,1S} = \frac{4i_{co}^{*1/3}}{f_0 s_{co}} e^{-s_{co}} = \frac{8\gamma_{co}}{3f_0 s_{co}^2} e^{-s_{co}} \tag{S45}$$

$$\theta_{d,1S} = \frac{4i^{*1/3}}{f_0(s_{co} - s_{cm})} e^{-s_{co}} = \frac{8\gamma_{mo}}{3f_0(s_{co} - s_{cm})^2} e^{-s_{co}} \tag{S46}$$

for 1S-nucleated crystals and droplets, respectively. Determined with our parameter values in Section S3, these $\theta_{c,1S}(s_{co})$ and $\theta_{d,1S}(s_{co})$ dependences are displayed in Fig. 7 of MT.

Similarly, for the delay time $\theta_{c,d,\infty}$ of nucleation of the crystals in bulk M-phase (macroscopically large droplet) we have $m^* = n^*$, $s = s_{cm}$ and, from eq. (S11), $f^* = g_0 e^{s_{cm}} n^{*2/3}$ so that eq. (S44) and the Gibbs-Thomson equation [1] $n^* = (2\gamma_{cm}/3s_{cm})^3$ lead to

$$\theta_{c,d,\infty} = \frac{4n^{*1/3}}{g_0 s_{cm}} e^{-s_{cm}} = \frac{8\gamma_{cm}}{3g_0 s_{cm}^2} e^{-s_{cm}}. \tag{S47}$$

This s_{co}-independent nucleation delay time is illustrated in Fig. 7a of MT.

S11. Effect of M on the nucleation delay times

The size effect due to our choice of $M = 240$ can be assessed at each supersaturation s_{co} by determining the various nucleation delay times at the smaller $M = 100$, 120, 160 and 200. Like the respective stationary nucleation rates, it turns out that none of the delay times θ_d, θ_{com}, θ_{d+com}, $\theta_{d+com+c}$, $\theta_{c,1S}$ and $\theta_{d,1S}$ is significantly affected by these M values. However, this is not so with θ_c and $\theta_{c,d}$. As seen in Fig. S7, both these delay times increase considerably with M, and the increase of $\theta_{c,d}$ is stronger at the smaller supersaturations.

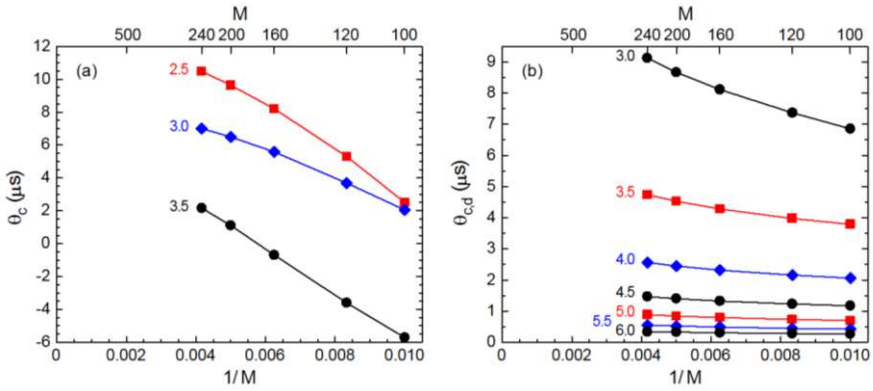

Figure S7. Dependence of the delay time θ_c of 2S crystal nucleation and the delay time $\theta_{c,d}$ of crystal nucleation in droplets on the maximum cluster size M used in solving the master equation of 2S nucleation, eq. (1) of MT. The symbols are our numerical data, the numbers indicate the supersaturations used in our study, and the lines are drawn to guide the eye.

S12. Chaotic growth of small subnucleus composites

When the subnucleus composites are sufficiently small, their growth can be very chaotic, because they necessarily follow very steep pathways up the energy hill in the physically accessible cluster size space. This is illustrated in Fig. S8 which represents the cluster flow lines near the origin of this space.

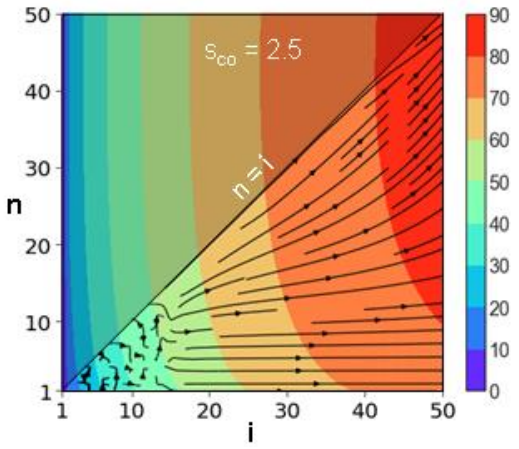

Figure S8. Cluster flow lines mandated by the fluxes from Eqs. (9)–(11) of MT in stationary 2S nucleation when $s_{co} = 2.5$ (then the peak of the energy hill is at $i = i^* = 78$ and $n = n^* = 42$, see Fig. 4a of MT). The arrow heads indicate the flow direction, and the background is the $w_{i,n}$ contour plot from Fig. 4a of MT. Only subnuclei of size i less than about 15 are in the zone of chaotic growth. The upper triangular part of the contour plot is obscure, because it is in the physically inaccessible i,n cluster size space. The $w_{i,n}$ scale is on the right of the figure.

References

[1] D. Kashchiev, J. Cryst. Growth **530** (2020) 125300.
[2] D. Kashchiev, *Nucleation: Basic Theory with Applications*, Butterworth-Heinemann, Oxford, 2000.
[3] D. Kashchiev, K. Sato, J. Chem. Phys. **109** (1998) 8530.
[4] D. M. Murphy, T. Koop, Q. J. R. Meteorol. Soc. **131** (2005) 1539.
[5] H. R. Pruppacher, J. D. Klett, *Microphysics of Clouds and Precipitation*, Kluwer, New York, 2004.
[6] R. Becker, W. Döring, Ann. Phys. (Leipzig) **24** (1935) 719.
[7] D. Kashchiev, J. Chem. Phys. **125** (2006) 044505.
[8] R. C. Miller, R. J. Anderson, J. L. Kassner, Jr., D. E. Hagen, J. Chem. Phys. **78** (1983) 3204.
[9] J. Wölk, R. Strey, J. Phys. Chem. B **105** (2001) 11683.
[10] Y. J. Kim, B. E. Wyslouzil, G. Wilemski, J. Wölk, R. Strey, J. Phys. Chem. A **108** (2004) 4365.
[11] V. Holten, D. G. Labetski, M. E. H. van Dongen, J. Chem. Phys. **123** (2005) 104505.